In-vitro studies of jet injections

Pankaj Rohilla, Jeremy O. Marston*

Department of Chemical Engineering, Texas Tech University, Lubbock, TX 79409, United States

ARTICLE INFO

ABSTRACT

In this study, needle-free jet injection dynamics were studied using homogeneous gelatin as model substrates. Whilst keeping nozzle properties such as orifice diameter (d_o) and ampoule volume (V) constant, we demonstrate the effect of standoff (s), confinement around the gel, storage modulus (G´) of model gel and liquid viscosity (μ) on the penetration depth of the jet injection. High-speed imaging was used to observe the liquid jet propagation and dispersion dynamics, whilst a load cell was implemented to measure the impact force for different standoff distance and viscosity of the liquid. The different parameters considered showed significant effects on penetration depth, with non-linear dependence on standoff being the key result, which may have implications for future injector designs. Moreover, the effect of confinement serves as a caution of using gelatin substrates as a proxy for human tissue.

1. Introduction

Using a high-speed jet to inject a drug through the skin is the oldest needle-free injection technique for transdermal vaccine delivery, dating back to the 1940's (Hingson and Hughes, 1947), and today needle-free jet injectors (NFJIs) are one of the effective alternatives to conventional needle injections, with multiple commercial devices cited in clinical trials (David et al., 2001; Yousafzai et al., 2017; Bavdekar et al., 2019). Needle phobia, injuries caused by needle-stick, and training for vaccine administration and safety are some of the challenges of needle-and-syringe injections (Mitragotri, 2005, 2006) and thus serve as some of the key drivers of NFJI technology. In particular, contraction of infectious diseases including hepatitis B virus (HBV), hepatitis C virus (HCV), and HIV are one of the biggest challenges (Mitragotri, 2005) faced by medical practitioners via hypodermic needles and syringe, thus necessitating a safe and robust drug delivery method.

On the other hand, minimal cross contamination (with disposable nozzles and spacers Brink et al., 1985), feasible self-administration, faster drug dispersion (Baxter, 2004) and immune response (Mitragotri, 2005) are some of the advantages of NFJIs. Yet despite the fact that jet injections for administering vaccines have been studied since 1940s (Hingson and Hughes, 1947), the physical mechanisms of this process are poorly understood, and it is therefore imperative to study the dynamics of jet injection.

In the jet injection process, a pressurized volume of liquid drug is expelled from a nozzle as a high-speed jet which penetrates the skin and deposits in the targeted region. Since jet injection must be able to target different regions, such as the dermis, sub-cutaneous, and intramuscular tissue, it is important to understand the mechanics and fluid dynamics of the jet injection for efficient delivery to a specified depth. The current hypothesis is that delivery to a specific region depends on the liquid properties, such as density (ρ) and viscosity (μ), jet velocity (v_j) and orifice diameter (d_o), which can be summarized by the jet power (Baxter and Mitragotri, 2005, 2006; Schoubben et al., 2015; Schramm-Baxter et al., 2004), given by $P = \frac{1}{8}\pi\rho d_o^2 v_j^3$.

In the literature, researchers have explored different actuation mechanisms to generate a steady and high speed jet. An orifice diameter in the range of $\approx$70–350 μm has been used to inject liquid with jet speeds of $\approx$60–200 m/s (Shergold et al., 2006; Moradiafrapoli and Marston, 2017). In designing a jet injection device, target depth into skin, jet shape and speed are crucial considerations for efficient delivery and minimization of the pain (Mitragotri, 2005; Arora et al., 2007; Park et al., 2015). Depending on the required volume, a jet injection device can be actuated with a spring-piston, compressed gas, thermo-cavitation, or piezoelectric mechanism (Shergold et al., 2006; Moradiafrapoli and Marston, 2017; Arora et al., 2007; Avila et al., 2015).

In understanding the fluid dynamics and mechanics of jet injection devices only a few studies are available in the literature (Schramm-Baxter et al., 2004; Shergold et al., 2006; Baker and Sanders, 1999; Ogunti and Popoola, 2014). At the same time, to assess the penetration dynamics, hydrogels and polymers have been used as model systems, due to tunable mechanical properties and hardness, which is in the same order as that of skin tissue (Schramm-Baxter et al., 2004; Shergold et al., 2006; Pailler-Mattei et al., 2008; Stachowiak et al., 2009). The

---

*Corresponding author.
E-mail address: jeremy.marston@ttu.edu (J.O. Marston).

effect of storage modulus of the model substrate, orifice diameter of the nozzle and actuation power on jet penetration and dispersion have been studied recently (Baker and Sanders, 1999; Schramm-Baxter and Mitragotri, 2004). However, parameters including standoff distance (s) between the skin surface and the orifice opening, liquid viscosity and hydrogel confinement have not been elucidated. As such their effect on the penetration and patterns of liquid dispersion inside the skin are poorly understood.

The objective of this study is to understand the effect of standoff, viscosity of jet, confinement and mechanical properties of the model gel. Substrates made from commercially available gelatin powders are used as the model gel due to similar order of hardness of human tissue and transparency to visualize the dispersion pattern of liquid injected, and a small spring-powered device is used to actuate the injection. Different hardness and storage modulus is tuned by changing the gelatin concentration in the gel. Three different standoff distances (0 mm, 15 mm and 30 mm) were used with liquids of different viscosity. Geometrical confinement is another parameter in the study, in which gel was molded in two tanks of different dimensions.

The reader should keep in mind that the results presented herein are not expected to translate directly to real animal or human tissue, be they ex-vivo or in vivo, since such tissues are heterogeneous and poroelastic matrices comprising multiple layers. Rather, the point here is that by using a homogeneous proxy, we can study factors such as standoff and viscosity in a controlled manner.

2. Materials and methods

2.1. Jet injector device

The NFJI used in this study was the spring powered Bioject® Intra-Dermal Pen (Inovio Pharmaceuticals), which could accommodate a reusable nozzle with orifice diameter of $\approx 156\,\mu m$ and transparent cartridge casing. Transparency of the cartridge and nozzle is crucial for tracking the plunger displacement in time during jet injection in order to derive volumetric flow rates, and thus the jet exit speed. The standoff distance between the nozzle orifice opening and the gelatin surface was varied from 0 mm to 30 mm. A liquid volume of 0.1 ml was ejected from the cartridge with the nozzle used. Fig. 1 shows the nozzle orifice and estimation of orifice diameter using a circle fitted on the orifice opening with image processing.

After manually cocking the spring-piston with an external lever, a pre-filled cartridge is locked into the ID Pen. The spring-piston is then activated by pressing an trigger ring, and the energy stored in the spring is converted into kinetic energy as the plunger travels through the cartridge and ejects liquid from the orifice as a jet. A portion of the kinetic energy of the ejected liquid was absorbed in the surface layer of the gelatin matrix on the impact. Inside the gelatin matrix, elastic forces opposes the inertial force of injected liquid and a balance between the two decides the ultimate penetration depth, volume injected and the dispersion pattern.
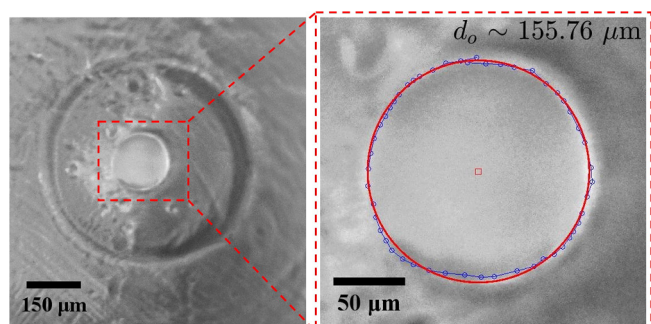
2.2. Materials used

Homogeneous gel substrates were prepared by mixing gelatin powder (*from bovine skin – 225 g Bloom, Type B, Sigma–Aldrich*) in Milli-Q water at a temperature of 65 °C with stirrer speed of 650 rpm. Gelatin solution was then poured into molds and kept in a refrigerator with a temperature of 5 ± 1 °C for 24 h. Gelatins of different stiffness were prepared with three different concentrations of gelatin (4%, 5% and 10% w/w) in water. A $5\%_{w/w}$ was chosen as a proxy for human tissue stiffness, whilst 4% and 10% were chosen to give stiffnesses of approximately a factor of two lower and an order of magnitude higher, respectively. Any concentration below 3% w/w gelatin gel (and concentrations below) was very soft and unsuitable for the study. To understand the effect of the confinement, gelatin hydrogel was prepared in two different tanks with dimensions of $9.7 \times 9.7 \times 50.17$ (mm³) and $64 \times 64 \times 70$ (mm³). Water, 50% glycerol and 80% glycerol were used as inject liquids for jet injections, with corresponding viscosities of $\mu = 1$ cP, 6.9 cP and 84 cP respectively, as measured using a rheometer (DHR3, TA Instruments), and densities $\rho = 1000$ kg/m³, 1123.75 kg/m³, and 1205.45 kg/m³ respectively at room temperature.

2.3. Mechanical characterization of the gelatin gel

Rheology of gelatin gels with different concentrations was performed to estimate the storage modulus in a rheometer (DHR2, TA Instruments). 25 mm parallel plate geometry was used with the gap of 750 μm with a temperature of 21 ± 1 °C. A custom made containment was used as a solvent trap with silicon oil filled around the meniscus of the gel sample between the parallel plates. After loading the sample between the parallel plates, time sweep tests (1% strain, 1 rad/s) were performed at a temperature of 21 ± 1 °C for a duration of 1.5 h. Strain amplitude sweep tests (1 rad/s, 0.01–10% strain) were performed on the gels to obtain the storage modulus. Storage modulus (G′) obtained for the 4%, 5% and 10% gelatin are 42.61 ± 31 Pa, 128.6 ± 53.17 Pa and 906.9 ± 151 Pa respectively and are presented in Fig. 2.

2.4. Impact force measurement

A miniature load button cell (Futek – LLB 130, 50 lb, Item # FSH03880) was placed beneath the orifice opening of the nozzle of the bioject device so that the liquid jet impinges on to the center of the button cell. The force measurements were made at a rate of 4800 samples per second for the duration of jet ($\sim 30 - 50$ ms). The load cell mechanism of the force measurement was based on a metal foil strain gauge. Applied compressive force on the button cell changes the resistance in metal foil inside the cell. An output signal corresponding to the applied force is recorded and logged. Three different standoff
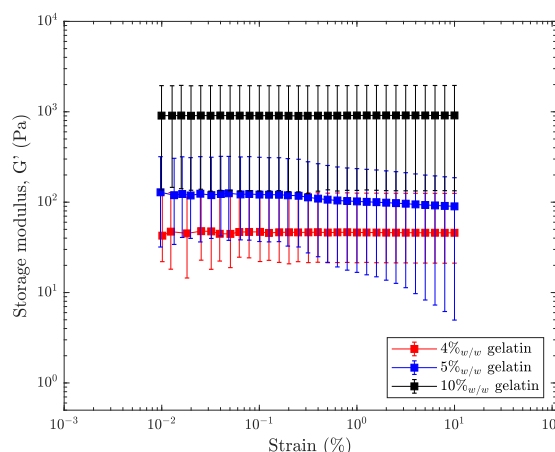

Fig. 1. Nozzle orifice and the estimated diameter ($d_o \approx 155.76 \pm 2\,\mu m$).

Fig. 2. Storage modulus, G′ for different concentrations of gelatin gels.

Fig. 3. Experimental setup (*Not scaled*).

(a) Plunger displacement with time

(b) Plunger motion for water (*Scale bar: 5 mm*)

Fig. 4. Plunger displacement with time for different liquids.
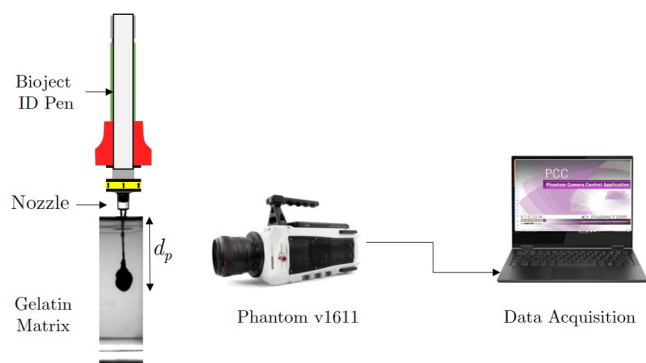

Fig. 5. Collimation of jet (a) Water (b) 50% Glycerol (c) 80% Glycerol *Scale bar: 4 mm.*

distances of $s = 2$ mm, 15 mm and 30 mm between the opening of nozzle orifice and button cell were used. Standoff distance of 2 mm was used instead of 0 mm because a small motion of bioject device in operation contributed additional force equivalent to the weight of the device to the measured force during the jet operation, resulting in erroneous force readings.

2.5. High speed imaging and motion analysis

In order to study the jet penetration and liquid dispersion pattern formation, high speed videography was used. A high speed camera (Phantom v1611) was used to capture the jet dynamics at a frame rate of 37,004 frames per second. The resolution used for the imaging was with exposure of 15 μs. Using a Nikon micro-Nikkor lens, the effective pixel resolution was in range of 130–200 μm/pixel. An LED panel and a diffuser sheet were placed in line with gel matrix and camera to achieve silhouette-type imaging and high contrast for image analysis. A Matlab script was used to track the plunger displacement and jet tip penetrating inside the gelatin substrate. The experimental setup used for the study is presented in Fig. 3.
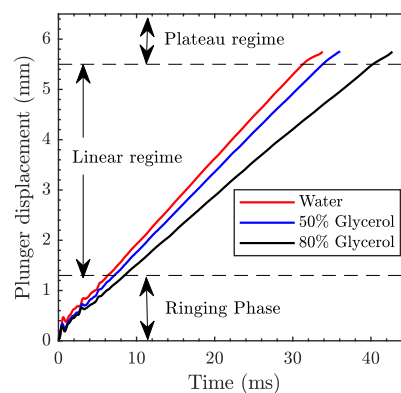
3. Results and discussions
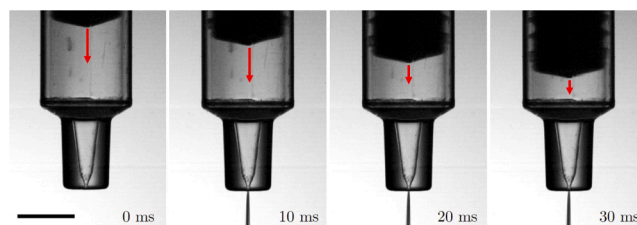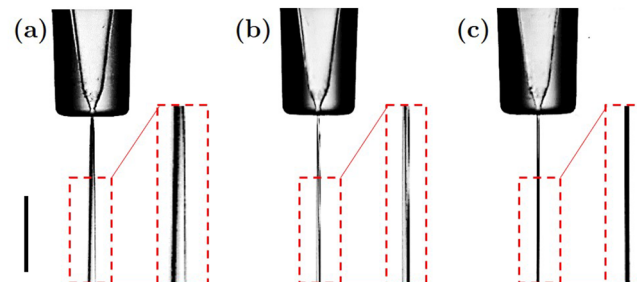
3.1. Jet characteristics

The liquid jet was characterized by the speed and coherency of the jet. Jet speed was estimated by tracking the plunger displacement in the transparent nozzle. Example displacement curves of the plunger with respect to the injection time are presented in Fig. 4. Three different regimes of plunger motion were identified as:- (1) Initial 'ringing' phase for time, $t \lesssim 5$ ms (due to plunger tip compressibility), (2) Linear flow regime and (3) Plateau regime in which flow diminishes and stopped ultimately. Assuming liquids to be incompressible, plunger speeds derived directly from the displacement were converted to jet speed for the linear regime using mass conservation. Estimated jet speeds (v_j) for water, 50% and 80% glycerol were 142.09 ± 1.03 m/s, 132.48 ± 2.07 m/s and 114.37 ± 0.94 m/s respectively.

To classify the nature of the jet flow, we estimated the Reynolds number (Re_j) for the liquid jets using orifice diameter ($d_o \approx 156$ μm) and average jet exit speed (v_j) as $Re_j = \rho d_o v_j \rho / \mu$. This gave values for water, 50% and 80% (w/w) glycerol of ≈21,944, ≈3333 and ≈251 respectively. These values are corroborated by a qualitative inspection of jet collimation, as presented in Fig. 5, where the turbulence is manifested by a dispersed jet stream for water (5(a)), and laminar flow by a collimated stream for 80% glycerol (5(c)). Likewise, the transitional flow for 50% glycerol (5(b)) appears to manifest by a jet that is in between the two limits.

As discussed earlier, jet power, P, offers one way to classify jet injection using a macroscopic energy balance (Schramm-Baxter and Mitragotri, 2004) with an assumption of constant velocity profile across the orifice as

$$P = \frac{1}{8} \pi \rho d_o^2 v_j^3.$$

The estimated jet power for water, 50% glycerol and 80% glycerol was ≈27.17 W, ≈24.53 W, and ≈16.51 W respectively. Jet speed, Reynolds number and power for the three fluids studied herein are summarized in Table 1 below.

3.2. Transient jet injection dynamics

To serve as a graphical supplement of the following discussion, we refer the reader to Fig. 6, which presents a sequence of select frames from a typical high-speed video. It is from these video sequences that

Table 1
Physical properties and jet parameters for the liquids used. The mixtures of water and glycerol were prepared as % w/w.

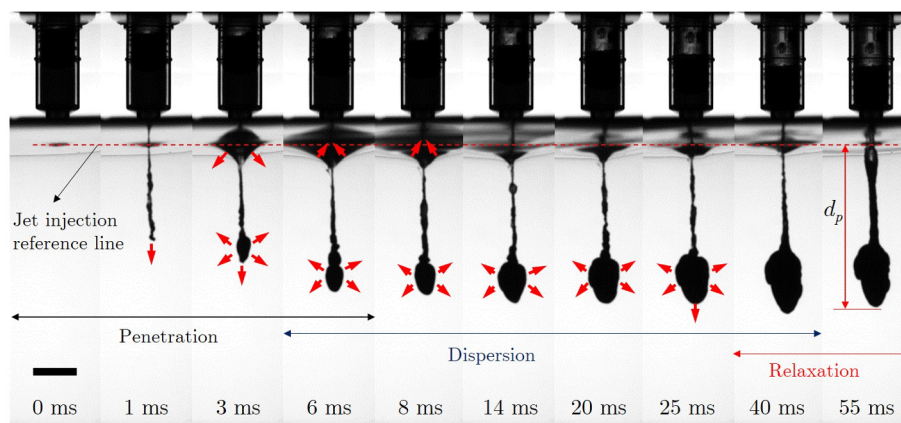| Liquid	Viscosity μ (cP)	Density ρ (kg/m^3)	Jet velocity v_j (m/s)	Reynolds # Re_j (–)	Power P (W)
Water	1	1000	142.09	21944	27.2
50% glycerol	6.9	1124	132.48	3333	24.5
80% glycerol	84	1205	114.37	251	16.5

Fig. 6. Jet propagation and dispersion of 50% glycerol in 5% w/w gelatin with zero standoff distance, $s = 0$. The scale bar is 8 mm.

the penetration depth of the injected liquid is measured and compared in order to understand the effect of different parameters. The penetration depth corresponds to the maximum depth achieved by the liquid after the injection ends and the gel structure relaxes.

In the first stage of injection, the liquid jets penetrate through the surface of gelatin forming a cylindrical channel. This stage of the process is usually very fast and lasts for only few milliseconds. In the second stage, resistive elastic force dominated the inertial jet force at the front tip of the jet in gelatin, and the incoming jet flow accumulates close to the depth of the hole, resulting in the formation of a three dimensional bolus as shown in Fig. 7. The time duration for the entire jet injection was in between 30 ms and 50 ms depending on the viscosity of the liquid.

To quantify the penetration dynamics, the motion of liquid jet tip inside the gelatin matrix was tracked for different combinations of the parameters used. A selection of these ensemble data sets are presented in Fig. 8 for the two confinements – namely – large tank (LT) and Cuvette, respectively (see Supplemental information). For each confinement, we explored the effect of gel % (w/w).

First and foremost, the data in Fig. 8 indicate a fundamental difference in penetration dynamics depending on the confinement. This is evident by comparison of figures (a–c) vs. (d–f), for the large tank and cuvette, respectively. The difference is quite stark and we observe that the penetration stage in the cuvette is rapid, lasting only 1–2 ms,
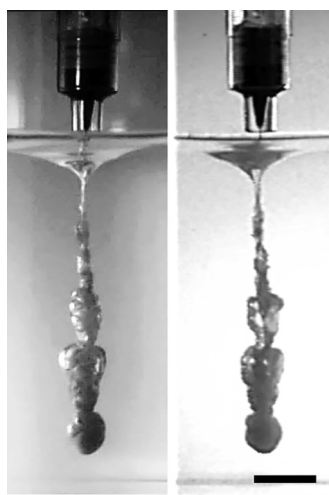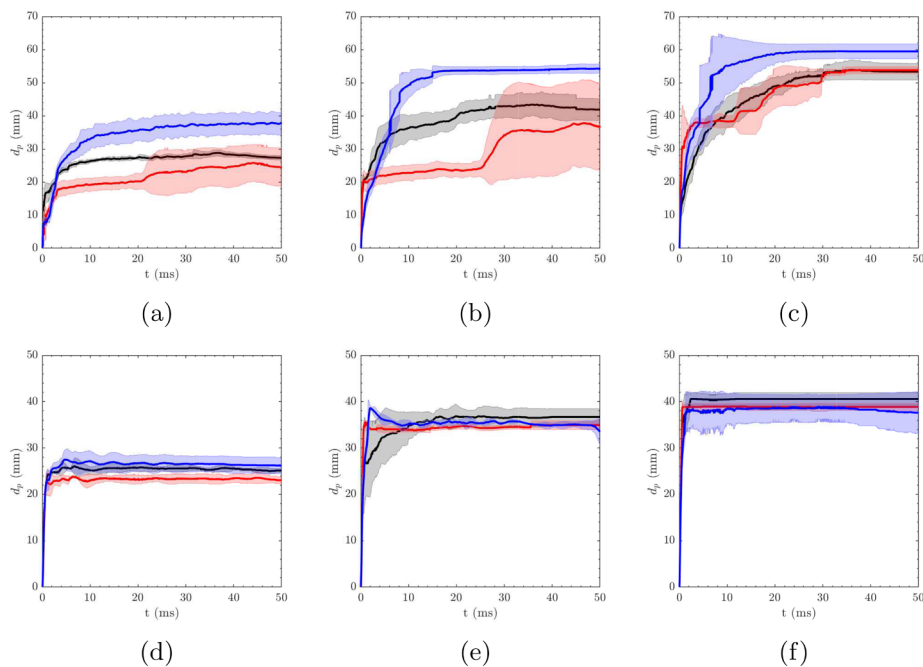
compared to a more gradual erosion for the large tank, which typically lasted up to 10 ms. Whilst we can also gauge from these curves that the standoff distance and viscosity influences the penetration depth, we reserve discussion of this for Section 3.3, and draw the reader's attention to a more subtle feature pertaining to dispersion phase.

Focusing first on the data for water and 50% glycerol in the large tank (Fig. 8a–c), the initial penetration stage occurs in a single-step fashion, followed by the dispersion stage. That is to say the maximum penetration depth is achieved before radial dispersion (see Fig. 9a). In contrast, by inspecting the same curves for 80% glycerol, we observe that the penetration-dispersion occurs in a multi-step process. In this case, a three dimensional bolus forms part way inside the gelatin as liquid deposits into the channel created by the jet penetration. At some point during this intermediate dispersion stage, the collimated jet stream for 80% glycerol propagates deeper in the gelatin, forming a secondary channel and another deeper bolus, as seen in Fig. 9b. We postulate that in the multi-step propagation, the collimated jet initially erodes the gel (frame at 1.4 ms), then is resisted by restorative elastic stresses in the gel at the tip of the jet. Combined with interaction between the jet stream and surrounding gel (i.e. inner wall surface of the cavity), this causes accumulation in the form of a liquid bolus (frame at 24.7 ms). As the incoming jet stream continues to interact with the existing eroded hole, the surrounding gel in the upper part forms a cavity and allows the jet to penetrate easily to the bottom of the bolus, whereupon the inertial force of the jet again erodes the gel locally and causes further penetration (frame at 29.2 ms). Competition between jet inertial force and gel elastic stress in the lower section of the cavity then cause the process to repeat and a secondary bolus is formed (frame at 65 ms). It is also important to note that the upper cavity is quite distinct from cavities observed in water-entry events since the cavity formed herein is due to fracture and erosion of the gelatin substrate and it is thus more robust to closure due to hydrodynamic pressure.

The multi-step process was only observed for the 80% glycerol in large tank configuration and thus we postulate that under strong confinement, factors such as viscosity and jet collimation are less significant. However, these factors play a stronger role in the unconfined large tank. The penultimate dispersion patterns (i.e. at maximal deformation) can vary depending upon the different parameters, and a summary of snapshots is presented in Fig. 10.

Lastly, at the conclusion of the dispersion stage, elastic stresses overcome inertial forces from the incoming jet stream and liquid in the bolus can flow back from the channel to the gelatin surface. This effect was more pronounced for the confined cuvette mold and thus, from the perspective of injected volume, the injection was less efficient for smaller confinements. When the gelatin relaxes, the three dimensional bolus shrinks and takes the shape of two-dimensional crack with negligible effect on final penetration depth.

Fig. 7. Three dimensional bolus resulting from fluid dispersion in the radial direction away from the jet flow. Left and right images correspond to orthogonal views from two synchronised cameras at time, t = 4.67 ms. *Scale bar: 8 mm.*

Fig. 8. Penetration depth with time for (a) 0 mm Standoff and 5% gelatin (LT), (b) 15 mm Standoff and 5% gelatin (LT), (c) 30 mm Standoff and 5% gelatin (LT), (d) 0 mm Standoff and 5% gelatin (Cuvette), (e) 15 mm Standoff and 5% gelatin (Cuvette), (f) 30 mm Standoff and 5% gelatin (Cuvette). *Liquids used: 50% Glycerol (━), 80% Glycerol (━), and Water (━), Shaded portions represent standard deviations..*
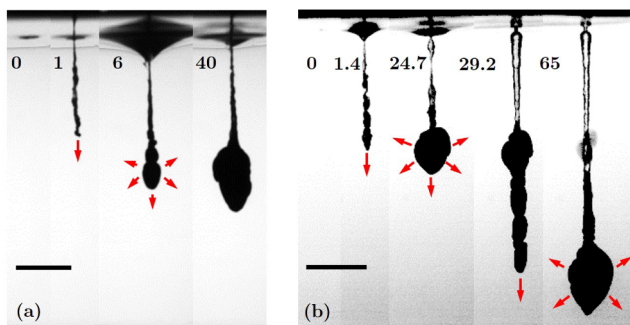
Fig. 9. Different propagation and dispersion mechanisms of injected liquid (a) Single-step propagation (50% Glycerol, 5% gelatin, 0 mm standoff), (b) Multiple-step propagation (80% Glycerol, 5% gelatin, 15 mm standoff) (*Time in ms, Scale bars: 10 mm*).
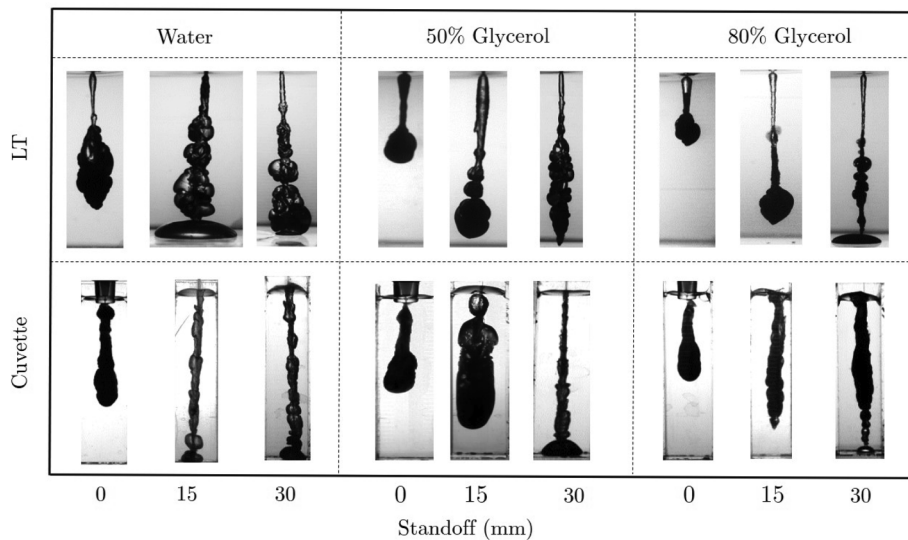
Table 2
Penetration depths (mm) in 5% w/w gelatin (LT) for different standoffs and viscosities.

Standoff s (mm)	Water $\mu = 1$ cP	50% glycerol $\mu = 6.9$ cP	80% glycerol $\mu = 84$ cP
0	38.40 ± 2.96	28.85 ± 1.19	24.45 ± 2.31
15	56.58 ± 1.48	43.20 ± 6.66	31.98 ± 14.58
30	61.26 ± 0.96	53.08 ± 6.62	55.61 ± 0.73

3.3. Penetration depth

Penetration depth, d_p, is defined as the maximum depth achieved by the liquid jet injected in gelatin matrix, and can be affected by standoff distance, gelatin concentration, viscosity and confinement. To exemplify the effect of standoff and viscosity, we single out the results for

Fig. 10. Dispersion patterns formed by liquid injected in 5% (w/w) gelatin.

(a) Water injection

(b) 50% Glycerol injection

(c) 80% Glycerol injection
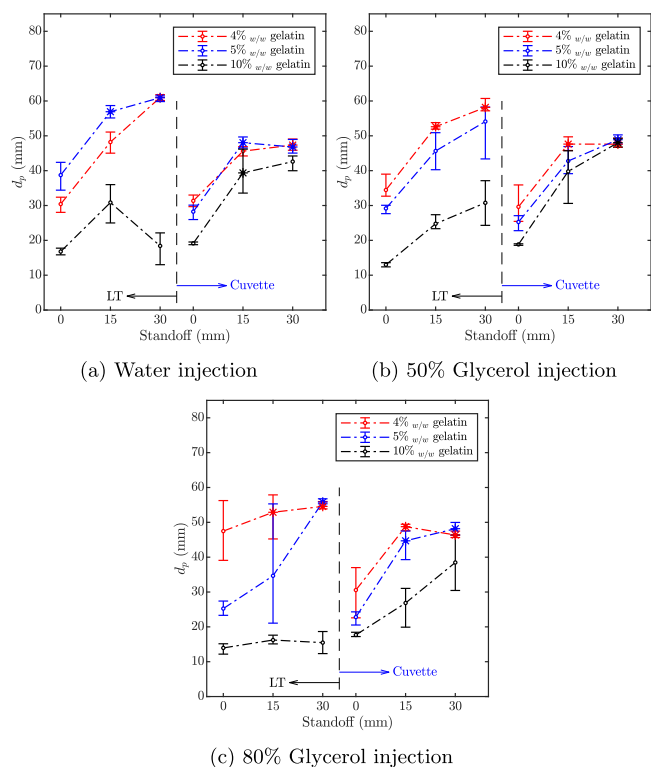
Fig. 11. Penetration depth obtained for different liquids injected in different gelatin substrates and standoff distances.

Fig. 12. Penetration depths for different standoffs for water injected in 10 % (w/w) gelatin.
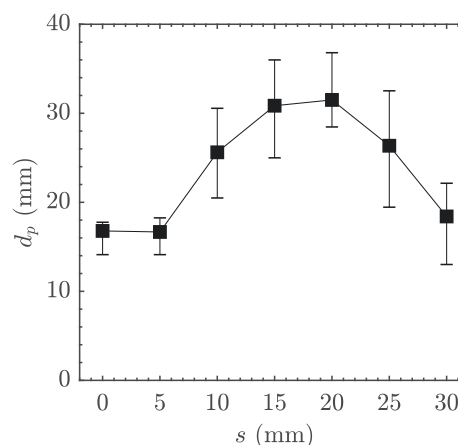
a fixed 5% gelatin and large tank, shown in Table 2. This data set indicates that penetration depth is an increasing function of standoff, but decreasing with viscosity.

The full spectrum of our data is presented in Fig. 11(a)–(c), segregated by liquids, from which we can infer different effects; In the case of zero standoff, smaller penetration depths were observed with increase in viscosity for both confinements. This decrease in penetration depth is consistent with the lower jet speeds for higher viscosities, however may also be compounded with increased shear stress acting on the jet due to interaction with the inner wall of the cavity (Tagawa et al., 2013), which is expected to increase linearly with viscosity. The penetration depth also decreases as the gel stiffness increases, which is intuitive as stiffer gels provide higher resistance to deformation, however, it should be noted this effect was more significant for the large tank as compared to smaller confinement.

The surprising, yet consistent result is increased penetration depths for increased standoff between the nozzle orifice opening and gelatin surface. This is counter-intuitive compared to the effects of viscosity and gel stiffness, since we expect the jet core velocity to diminish with increasing distance from the orifice. We hypothesize that there are two factors that contribute to this result; first, the force of the jet pushes the gel away from the orifice forming a cusp-like dent at the surface level (see Figs. 6 and 7), which relaxes throughout the injection. As such there may be some interplay between the gel surface and orifice that disrupts the stream for $s = 0$ mm, as opposed to stand-offs of 15 and 30 mm. Secondly, jet dispersion implies a larger footprint at the gel surface, which could result in a larger hole at the surface, making it easier for subsequent jet flow to penetrate. This second factor appears to be supported by images in Figs. 9 and 10.

The exception to this, and even more surprising, is for water jets into 10% (w/w) gelatin in large tank where the depth appears to exhibit a maxima with respect to standoff; this important observation led us to perform additional experiments covering the standoff range 0–30 mm in finer increments, discussed in more detail in Section 3.4.

In the case of 50% glycerol, monotonic increase in penetration

depth was observed for increase in standoff distance from 0 mm to 15 mm. The effect of increasing standoff to 30 mm showed an increase in depth in larger confinement, whereas no significant change was seen in smaller confinements for the same concentrations of the gelatin. For 80% glycerol, despite observing a collimated laminar jet flow (see Section 3.1), the data trends were not as consistent, which we propose is due to the multi-step penetration/dispersion process. This physical feature is manifested by larger error bars in the data.

3.4. Critical standoff

As noted in Fig. 11a, for the specific combination of the lowest viscosity (water) in the stiffest gel (10% w/w), we observed a striking feature of depth vs. standoff during our principal study – namely – a peak penetration depth of $d_p \approx 31$ mm, occurring for $s = 15$ mm. To investigate this further, the standoff distance was varied from 0 mm to 30 mm, in increments of 5 mm and the total depth was again recorded. The full results of this procedure are shown in Fig. 12. Standoffs of $s = 0$ and 5 mm showed no difference. However by increasing the standoff from $s = 5 \rightarrow 20$ mm, the penetration depth gradually increases from $d_p = 17$ to 32 mm. Further increasing the standoff from 20 to 30 mm resulted in decreased penetration depth, and we note that at $s = 30$ mm, the depth is almost the same as for $s = 0$ mm. As such, the depth exhibits a local maxima around $s = 15$–20 mm. This non-linear dependence has not (to our knowledge) been reported previously in the context of jet injections. The only previous report that the authors are aware of where the jet standoff was found to have a non-linear effect is that in Sittiwong et al. (2010). In their study, water jets with speeds up to ~ 2 km/s emanated from orifice of 700 μm and impacted a pressure sensor. The resulting impact pressure, on the order of 1–3 GPa, exhibited a maxima for a standoff around 30–40 mm.

The fact that standoff distance can alter the penetration depth was first observed in 1947 (Hingson and Hughes, 1947) and has been known to manufacturers (Mohammed et al., 2010), however, the full extent of the relationship is clearly not well-defined. Elucidating this relationship and the interaction between standoff and viscosity is therefore paramount as it may have implications for future design of injectors targeting different tissues.

3.5. Force measurements

To gain further insight into the physics behind the critical standoff distance, impact forces were measured for different liquids impinging on a load cell from different standoffs. Three standoff distances of 2 mm, 15 mm and 30 mm were used between the load cell and the nozzle tip, since zero stand-off cannot be implemented with the force
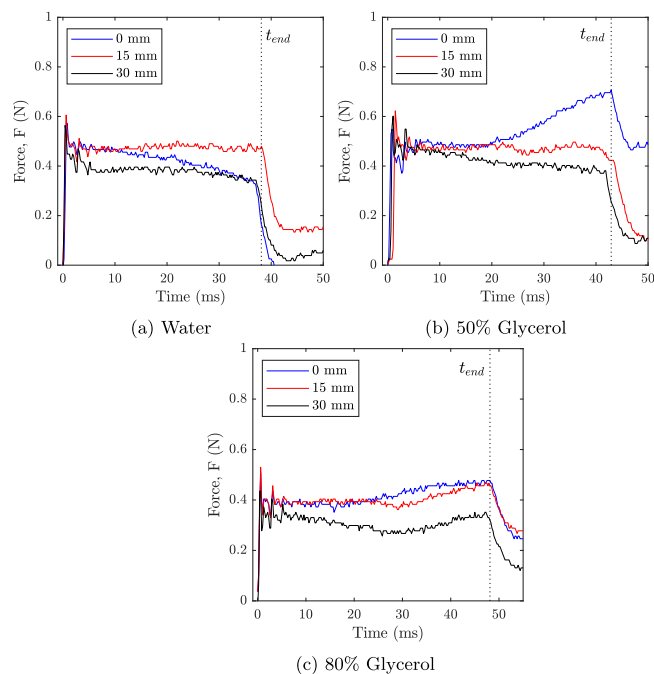
(a) Water

(b) 50% Glycerol

(c) 80% Glycerol

Fig. 13. Force Measurements for (a) 2 mm standoff, (b) 15 mm standoff and (c) 30 mm standoff. Dashed line represents the time, t_{end} where the injection ends.

sensor. The impact forces measured for different liquids are presented in Fig. 13. The early-time data ($t \lesssim 5$ ms) in the force-time curves mirror the displacement curves in Fig. 4(a) with a distinct 'ringing' phase where the force oscillates. This is due to compression of both the rubber plunger tip and liquid, caused by the sudden impulse of the spring-piston. This over-pressure inside the cartridge manifests in a peak impact force, F^*, prior to the linear motion. For water and 50% glycerol, We observe $F^* \approx 0.6$ N, whilst for 80% glycerol $F^* \approx 0.4 - 0.5$ N. The subsequent dynamic force, F, can then exhibit one of three trends – (i) impact force, F remains more-or-less constant until the end of injection (e.g. water with $s = 15$ mm), (ii) F gradually decays until the end of the injection (e.g. water with $s = 0$ mm), or (iii) F initially decays slightly, but then increases in the latter part of injection (e.g. 80% glycerol).

In previous studies, the force has been used as the primary verification of jet speed (Schoubben et al., 2015; Mohizin et al., 2018) by assuming that the force is attributed to the inertial pressure of the jet, $\sim \rho v_j^2$, multiplied by the cross-sectional area (Uth and Deshpande, 2013), typically taken to be $A_o = \frac{\pi}{4} d_o^2$. Using the approximation $F = \rho v_j^2 A_o$, we find $F \approx 0.38$ N, 0.37 N, and 0.29 N for water, 50% glycerol and 80% glycerol, respectively. These values are on the same order of magnitude as the measured forces in Fig. 13, however, they do not depict the true trends observed in the force curves, nor can they explain the trends in Section 3.3 for penetration depth. The primary flaw is the assumption of constant area, A_o, which is not valid for turbulent jets as per our observations of the jet in Fig. 5. The velocity distribution for non-zero stand-off must also be considered.

Possible explanations for the trends seen in the force curves and gel penetration are as follows: The centerline velocity, U_m, in the case of laminar jets in air is expected to decay as $U_m \propto Re_o v_j d_o / s$, where s is the downstream distance from the orifice (stand-off) (Gauntner et al., 1970). The mean force, $\overline{F} \sim U_m^2$, in the linear stage for both 50% and 80% glycerol does in fact decrease with stand-off. The penetration depth however, was found to increase with stand-off, which we believe is due to a confluence of relaxation of the gel surface itself (more pronounced at low stand-offs) and larger hole diameter (for higher stand-offs) enabling the jet flow to penetrate with less interaction with the surrounding gel.

In contrast, for turbulent jets, experimental measurements indicate

that the core length wherein $U_m = v_j$ can persist for up to a critical distance, s^* of 100 orifice diameters (Rajaratnam and Albers, 1998), i.e. $s^* \approx 100 d_o$. After this critical distance, the center-line velocity was found decaying linearly with distance, i.e. $U_m \propto v_j / s$ for $s > s^*$. The velocity distribution is also expected to follow a Gaussian, $U(r) = U_m exp(-\kappa r^2 / s^2)$, meaning a reduced velocity toward the edge of the jet, where κ is a constant and r is the radius of the jet. Lastly, turbulent jets also disperse with a cone angle of approximately 1° for water, leading to jet diameters of about 600–700 μm for $s = 15$–20 mm. As such, noting that $s^* \approx 15$ mm for our system, this stand-off distance may represent an optimum in terms of minimal velocity decay coupled with a slightly larger impact area, leading to a higher impact force and maximal penetration depth for the stiff gel ($10\%_{w/w}$). This argument is supported by the force measurements for water, seen in Fig. 13. For the weaker gels, where deformation is more pronounced, we again propose that both the gel surface movement and the wider hole (due to jet dispersion) contribute to increased penetration depths.

Again, we highlight the fact that these results, as with many previous studies, pertain strictly to in vitro assessments and that the trends with regards to stand-off will not necessarily be observed for ex-vivo or in vivo studies since true human or animal tissues are multi-layered, heterogeneous and poro-elastic in nature. Elucidating the confluence of viscosity and stand-off for such tissues is the subject of on-going work and will be addressed in detail in subsequent publications.

4. Conclusions

In summary, we have conducted a study of jet injection into gelatin substrates, with the principal control parameters being orifice stand-off distance (s), fluid viscosity (μ), gel stiffness and geometrical confinement. Both the gel stiffness and confinement were shown to have a strong influence on the penetration, which therefore needs to be considered in evaluating existing and future in vitro studies. Jet penetration showed a significant dependence on liquid viscosity and gelatin strength, which was more prominent in larger confinement as compared to smaller confinement.

A key factor in our study, which has been largely overlooked in previous studies is the effect of stand-off. For most viscosity-standoff combinations, increasing standoff resulted in increased penetration depth which is proposed to result from factors such as jet dispersion and deflection and relaxation of the gel surface. However, one key observation made for water with the stiffest gel was a local maxima in penetration depth which occurred for a stand-off of approximately 15–20 mm, which was consistent with impact force measurements. We propose this result must be interpreted in the context of velocity distribution and dispersion of turbulent jets.

As a final remark, we note that whilst dynamics in homogeneous substrates can reveal the significance of individual factors, they do not necessarily represent those in true tissue, which are heterogeneous and poroelastic.

Declaration of Competing Interest

None.

Appendix A. Supplementary data

Supplementary data associated with this article can be found, in the online version, at https://doi.org/10.1016/j.ijpharm.2019.118503.

References

Hingson, Robert A., Hughes, James G., 1947. Clinical studies with jet injection: a new method of drug administration. Anesthesia Analgesia 26 (6), 221–230.

Bremseth, David L., Pharm, D., Pass, Franklin, 2001. Delivery of insulin by jet injection: recent observations. Diabetes Technol. Therap. 3 (2), 225–232.

Yousafzai, Mohammad Tahir, Saleem, Ali Faisal, Mach, Ondrej, Baig, Attaullah, Sutter, Roland W., Zaidi, Anita K.M., 2017. Feasibility of conducting intradermal vaccination campaign with inactivated poliovirus vaccine using tropis intradermal needle free injection system, Karachi, Pakistan. Heliyon 3 (8), e00395.

Bavdekar, Ashish, Malshe, Nandini, Ravichandran, Latha, Sapru, Amita, Kawade, Anand, Lalwani, Sanjay, Palkar, Sonali, Hanumante, Neeta, Gunale, Bhagwat, Kapse, Dhananjay, et al., 2019. Clinical study of safety and immunogenicity of pentavalent dtp-hb-hib vaccine administered by disposable-syringe jet injector in india. Contemp. Clin. Trials Commun. 14, 100321.

Mitragotri, Samir, 2006. Current status and future prospects of needle-free liquid jet injectors. Nat. Rev. Drug Discov. 5 (7), 543.

Mitragotri, Samir, 2005. Immunization without needles. Nat. Rev. Immunol. 5 (12), 905.

Brink, P.R.G., Van Loon, M., Trommelen, J.C.M., Gribnau, W.J., Smale-Novakova, I.R.O., 1985. Virus transmission by subcutaneous jet injection. J. Med. Microbiol. 20 (3), 393–397.

Baxter, Joy Rene, 2004. Fundamental Mechanisms of Drug Delivery by Jet Injection: Basis for the Development of a Painless Microject Injector. University of California, Santa Barbara.

Baxter, Joy, Mitragotri, Samir, 2006. Needle-free liquid jet injections: mechanisms and applications. Expert Rev. Med. Devices 3 (5), 565–574.

Baxter, Joy, Mitragotri, Samir, 2005. Jet-induced skin puncture and its impact on needle-free jet injections: experimental studies and a predictive model. J. Control. Release 106 (3), 361–373.

Schoubben, Aurélie, Cavicchi, Andrea, Barberini, Lanfranco, Faraon, Alessio, Berti, Marco, Ricci, Maurizio, Blasi, Paolo, Postrioti, Lucio, 2015. Dynamic behavior of a spring-powered micronozzle needle-free injector. Int. J. Pharm. 491 (1–2), 91–98.

Schramm-Baxter, Joy, Katrencik, Jeffrey, Mitragotri, Samir, 2004. Jet injection into polyacrylamide gels: investigation of jet injection mechanics. J. Biomech. 37 (8), 1181–1188.

Shergold, Oliver A., Fleck, Norman A., King, Toby S., 2006. The penetration of a soft solid by a liquid jet, with application to the administration of a needle-free injection. J. Biomech. 39 (14), 2593–2602.

Moradiafrapoli, M., Marston, J.O., 2017. High-speed video investigation of jet dynamics from narrow orifices for needle-free injection. Chem. Eng. Res. Des. 117, 110–121.

Arora, Anubhav, Hakim, Itzhak, Baxter, Joy, Rathnasingham, Ruben, Srinivasan, Ravi, Fletcher, Daniel A., Mitragotri, Samir, 2007. Needle-free delivery of macromolecules across the skin by nanoliter-volume pulsed microjets. Proc. Natl. Acad. Sci. 104 (11), 4255–4260.

Park, Geehoon, Modak, Ashin, Catherine Hogan, N., Hunter, Ian W., 2015. The effect of jet shape on jet injection. In: 37th Annual International Conference of the IEEE Engineering in Medicine and Biology Society (EMBC). IEEE, pp. 7350–7353.

Avila, Silvestre Roberto Gonzalez, Song, Chaolong, Ohl, Claus-Dieter, 2015. Fast transient microjets induced by hemispherical cavitation bubbles. J. Fluid Mech. 767, 31–51.

Baker, Aaron B., Sanders, Joan E., 1999. Fluid mechanics analysis of a spring-loaded jet injector. IEEE Trans. Biomed. Eng. 46 (2), 235–242.

Ogunti, Erastus O., Popoola, Olaoluwa R., 2014. Fluids mechanics analysis of voice coil needle free jet injector. Adv. Phys. Theor. Appl. 34, 60.

Pailler-Mattei, C., Bec, S., Zahouani, H., 2008. In vivo measurements of the elastic mechanical properties of human skin by indentation tests. Med. Eng. Phys. 30 (5), 599–606.

Stachowiak, Jeanne C., Li, Thomas H., Arora, Anubhav, Mitragotri, Samir, Fletcher, Daniel A., 2009. Dynamic control of needle-free jet injection. J. Control. Release 135 (2), 104–112.

Schramm-Baxter, Joy, Mitragotri, Samir, 2004. Needle-free jet injections: dependence of jet penetration and dispersion in the skin on jet power. J. Control. Release 97 (3), 527–535.

Tagawa, Yoshiyuki, El Nikolai, A., Galbzuori, Oudalov, Lohse, Detlef, 2013. Needle-free injection into skin and soft matter with highly focused microjets. Lab Chip 7, 1357–1363.

Sittiwong, Wuttichai, Seehanam, Wirapan, Pianthong, Kulachate, Matthujak, Anirut, 2010. Effect of stand-off distance on impact pressure of high speed water jets. In: AIP Conference Proceedings. AIP, pp. 864–873 vol. 1225.

Mohammed, Ali Jafer, AlAwaidy, Salah, Bawikar, Shyam, Kurup, Padmamohan J., Elamir, Emadaldin, Shaban, Mahmoud M.A., Sharif, Sharif M., van der Avoort, Harrie G.A.M., Pallansch, Mark A., Malankar, Pradeep, 2010. Fractional doses of inactivated poliovirus vaccine in oman. N. Engl. J. Med. 362 (25), 2351–2359.

Mohizin, Abdul, Reby Roy, K.E., Lee, Donghee, Lee, Seung Ku, Kim, Jung Kyung, 2018. Computational fluid dynamics of impinging microjet for a needle-free skin scar treatment system. Comput. Biol. Med. 101, 61–69.

Uth, Tobias, Deshpande, Vikram S., 2013. Unsteady penetration of a target by a liquid jet. Proc. Natl. Acad. Sci. 110 (50), 20028–20033.

Gauntner, James W., Hrycak, P., Livingood, J.N.B., 1970. Survey of literature on flow characteristics of a single turbulent jet impinging on a flat plate. NASA Technical Reports Server.

Rajaratnam, N., Albers, C., 1998. Water distribution in very high velocity water jets in air. J. Hydraul. Eng. 124 (6), 647–650.